European Journal of Radiology 116 (2019) 144–149

Contents lists available at ScienceDirect

European Journal of Radiology

journal homepage: www.elsevier.com/locate/ejrad

Research article

Clinically significant prostate cancer detection on MRI: A radiomic shape features study

Renato Cuocolo[a], Arnaldo Stanzione[a,*], Andrea Ponsiglione[a], Valeria Romeo[a], Francesco Verde[a], Massimiliano Creta[b], Roberto La Rocca[b], Nicola Longo[b], Leonardo Pace[c], Massimo Imbriaco[a]

[a] Department of Advanced Biomedical Sciences, University of Naples "Federico II", Naples, Italy
[b] Department of Neurosciences, Reproductive Sciences and Odontostomatology, University of Naples "Federico II", Naples, Italy
[c] Department of Medicine and Surgery, University of Salerno, Salerno, Italy

ARTICLE INFO

Keywords:
MRI
Radiomics
Shape
Prostate cancer
Gleason score

ABSTRACT

Purpose: Prostate multiparametric MRI (mpMRI) is the imaging modality of choice for detecting clinically significant prostate cancer (csPCa). Among various parameters, lesion maximum diameter and volume are currently considered of value to increase diagnostic accuracy. Quantitative radiomics allows for the extraction of more advanced shape features. Our aim was to assess which shape features derived from MRI index lesions correlate with csPCa presence.

Materials and Methods: We retrospectively enrolled 75 consecutive subjects, who underwent mpMRI on a 3 T scanner, divided based on MRI index lesion Gleason Score in a csPCa group (GS > 3 + 4, n = 41) and a non-csPCa one (n = 34). Ten shape features were extracted both from axial T2-weighted and ADC maps images, after lesion tridimensional segmentation. Univariable and multivariable logistic analysis were used to evaluate the relationship between shape features and csPCa. Diagnostic performance was assessed measuring the area under the curve of the receiver operating characteristic (ROC) analysis. Diagnostic accuracy, sensitivity, and specificity were determined using the best cut-off on each ROC. A P value < 0.05 was considered statistically significant.

Results: Univariable analysis demonstrated that almost every shape feature was statistically significant between csPCa e non-csPCa groups. However, multivariable analysis revealed that the parameter defined as surface area to volume ratio (SAVR), especially when extracted from ADC maps is the strongest independent predictor of csPCa among tested shape features.

Conclusion: The radiomic shape feature SAVR, extracted from ADC maps after index lesion segmentation, appears as a promising tool for csPCa detection.

1. Introduction

Prostate cancer (PCa) has the highest prevalence among malignancies affecting men and is a leading cause of cancer related deaths in the United States [1]. Over the last decade, PCa screening, performed with serum levels of prostate-specific antigen (PSA) testing and systematic prostate biopsies, has reduced both the incidence of advanced PCa and PCa mortality [2]. Nevertheless, this approach leads to over-diagnosis and consequently over-treatment of low-risk and indolent PCa, with significant implications in terms of patient care [3,4]. Indeed, the mortality of PCa greatly varies according to various factors and in particular Gleason score (GS), which is of great importance in the stratification of risk for PCa patient [5,6].

In this setting, multiparametric MRI (mpMRI) of the prostate has been proposed as a triage test to reduce unnecessary biopsies and over-diagnosis of clinically insignificant PCa, defined as GS < 4 + 3 or as maximum cancer core length < 6 mm [7]. The very aim of mpMRI is to identify index lesions inside the prostatic gland with a high probability of clinically significant prostate cancer (csPCa) [8]. In the current PI-RADSv2 guidelines, lesion measurement is performed by reporting the largest dimension on the axial plane, with possible addition of the largest dimension on sagittal and/or coronal images and volume

Abbreviations: PCa, prostate cancer; PSA, prostate-specific antigen; GS, Gleason score; mpMRI, multiparametric MRI; csPCa, clinically significant prostate cancer; TRUS, transrectal ultrasound; VOI, volume of interest; AUC, area under the curve; ROC, receiver operating characteristic; T2w, T2 weighted; SAVR, surface area to volume ratio; DCE, dynamic contrast enhanced

* Corresponding author at: Department of Advanced Biomedical Sciences, University of Naples "Federico II", Via S. Pansini, 5, 80131, Naples, Italy.
E-mail address: arnaldo.stanzione@unina.it (A. Stanzione).

https://doi.org/10.1016/j.ejrad.2019.05.006
Received 21 March 2019; Received in revised form 2 May 2019; Accepted 6 May 2019

calculation using the ellipsoid formula. A lesion volume ≥ 0.5 cc in mpMRI is suggestive of csPCa. Despite mpMRI being a powerful diagnostic tool, its interpretation can be challenging and it could still be missing a relatively low percentage of csPCa [9,10]. Several strategies are currently investigated to further increase the diagnostic accuracy of mpMRI in the detection of csPCa, such as the combination of imaging and laboratory tests, although results are still conflicting in literature [11,12]. Other proposed approaches focus on quantitative analysis of MR images and appear promising [13]. In a recent paper, Tamada et al. showed in a large cohort of patients that diffusion kurtosis did not show a clear added value compared with conventional diffusion weighted imaging methods for clinical prostate cancer evaluation [14]. Of great interest is the field of radiomics, the conversion of medical images into high-dimensional data [15]. Radiomic approaches have been proposed in order to identify the presence of disease on MRI and also to non-invasively grade, stage and stratify disease risk [16–20]. Among the extractable features are those tied to lesion shape. These are descriptors of region of interest size and shape in the three dimensions, and contrary to other radiomic data, they are independent from gray level value distribution, potentially allowing for greater reproducibility [21]. A recent study by Krishna et al. explored the diagnostic value of radiomic shape features in the discrimination between benign prostate hyperplasia and PCa in the transitional zone, with encouraging results [22].

As tumor size has been related to aggressiveness of PCa [8,23], the purpose of this study was to evaluate whether radiomic shape features derived from MR images could be effective in csPCa identification, using target prostate biopsy or radical prostatectomy as the reference standard.

2. Materials and methods

This retrospective study was approved by the local Institutional Review Board and the need for written informed consent was waived.

2.1. Patient population

All exams of consecutive patients who underwent prostate mpMRI at our Institution, based on current clinical guidelines between June 2016 and March 2018 (n = 198), were reviewed [5]. Patients were excluded if no suspicious index lesion were identified at mpMRI (PI-RADSv2 score < 3, n = 72), if they did not undergo targeted biopsy or radical prostatectomy within 3 months of the exam (n = 24), if they had incomplete or inadequate (e.g. presence of artifacts) images (n = 7) or in case histopathological confirmation of PCa (GS ≥ 3 + 3) in the MRI index lesion was unavailable (n = 20). A urologist, with 5 years of experience in performing cognitive MRI targeted transrectal ultrasound-guided (TRUS) biopsies, was responsible for sampling at least two cores from the index lesion in addition to standard 12-core systematic TRUS biopsy. A detailed description of the biopsy procedure has been previously reported [12]. Based on index lesion GS, two groups were identified: csPCa (GS > 3 + 4) and non-csPCa groups. A flow chart of patient selection is shown in Fig. 1.

Table 1
Technical parameters of each MRI sequence included in the multiparametric MRI protocol.

	Axial DWI	*Axial T2w*	*Sagittal T2w*	*Coronal T2w*	*DCE*
TR (ms)	4900	4000	4000	4000	4.38
TE (ms)	89	101	101	101	1.55
Slice thickness (mm)*	3	3	3	3	3
Matrix	144 × 144	310 × 320	310 × 320	310 × 320	115 × 192
FOV (mm)	200 × 200	200 × 200	200 × 200	200 × 200	260 × 260

DWI: Diffusion Weighted Imaging; DCE: Dynamic Contrast Enhanced; T2w: T2-weighted; TR: repetition time; TE: echo time; FOV: field of view.
DWI was performed with b values of 50, 800 and 1500sec/mm$^{2.}$
DCE temporal resolution was 6 s and total acquisition time was.4 min
*no gap between slices.

2.2. MRI data acquisition and image analysis

The mpMRI acquisition protocol performed on a 3 T scanner (Magnetom Trio, Siemens Healthcare, Erlangen, Germany) without endorectal coil followed PI-RADSv2 recommendations has been previously reported (Table 1) [8,20]. Two readers trained in urogenital imaging reviewed axial T2-weighted (T2w), DWI and ADC map images of included patients identifying index lesions in accordance to PI-RADSv2 guidelines. Subsequently, working in consensus, they annotated images from both T2w and ADC maps by drawing polygonal regions of interest on each slice in which the index lesion was visible, generating a volume of interest (VOI), using a dedicated software (ITKSnap, v3.6.0) (Fig. 2) [24]. In case of discordance a third, senior, radiologist reviewed the images to reach a final agreement.

The extracted VOIs were then analyzed with an open-source package for quantitative data extraction from medical images (Pyradiomics, v2.1.2) [25]. In particular, ten shape parameters were recorded from each T2w and ADC map VOIs (Table 2). In detail, these were derived from the approximated triangle mesh of the VOIs, built by vertices placed halfway on the edge between voxels inside and outside the segmentation mask, subsequently connected forming triangles of three adjacent vertices [21].

2.3. Statistical analysis

Data were tested for normal distribution by the Kolmogorov-Smirnov test and expressed as mean ± standard deviation or as median and range, as appropriate. Univariable logistic analysis was used to assess the relationships between shape features and group classification. Thereafter, only features found significant at univariable

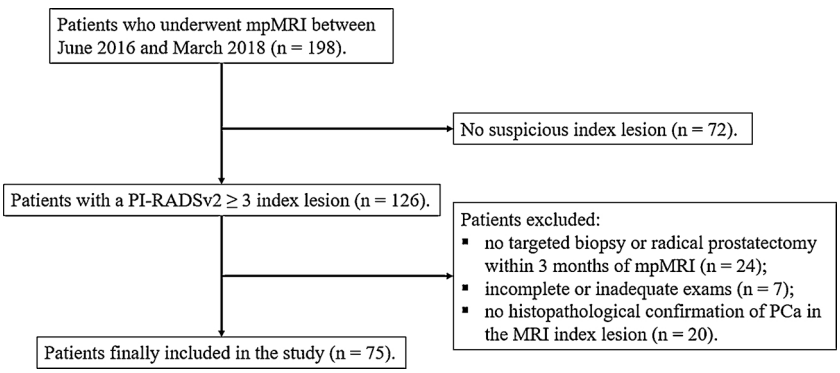

Fig. 1. Flow chart illustrating the patient selection process.

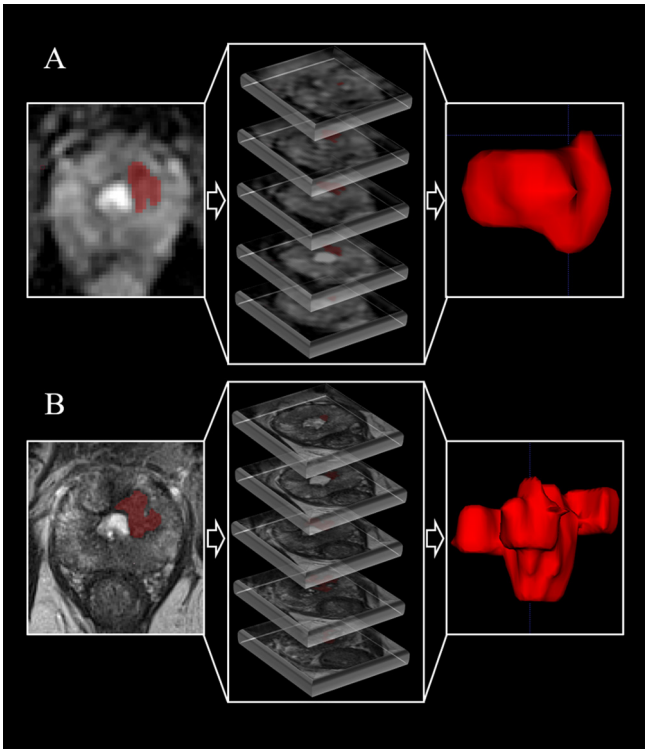

Fig. 2. An example of image annotation performed on the ADC map (A) and T2w (B) images of a patient with low Gleason Score prostate cancer (3 + 3) located in the left mid gland transitional zone. On the right, the corresponding volumetric representation of the region of interest is shown.

logistic analysis were entered in the multivariable logistic analysis. The diagnostic performance of each shape feature was assessed measuring the area under the curve (AUC) of the receiver operating characteristic (ROC) analysis [26]. AUC differences among parameters were analyzed using the Hanley-McNeil method. Diagnostic accuracy, sensitivity, and specificity, with corresponding 95% confidence intervals, were determined using the best cut-off on each ROC. A p value < 0.05 was considered statistically significant. MedCalc Statistical Software version 13.1.2 was used for statistical analysis.

3. Results

A total of 75 patients were finally included in our study with their clinical parameters reported in Table 3. Of these, 41 belonged to the csPCa group and 34 to the non-csPCa one.

At univariable analysis, all variables derived from T2w images were significant (Table 4), while at multivariable analysis the surface area to volume ratio (SAVR) was the only significant predictors of csPCa (O.R. 0.0102, 95% C.I. 0.0009 to 0.1197, $p < 0.0001$). Of all the variables obtained from ADC map images, only differences in elongation and flatness derived from the ADC map VOIs did not result statistically significant (Table 5), while at multivariable analysis, SAVR was the only significant predictor (O.R. 0.0098, 95% C.I. 0.009 to 0.1073, $p < 0.0001$). Fig. 3 shows a graphical representation of SAVR distribution in the study population. This parameter is calculated as follows from the VOI triangle mesh:

$$\frac{\sum_{i=1}^{N_f} \frac{1}{2} |a_i b_i \times a_i c_i|}{\sum_{i=1}^{N_f} \frac{Oa_i \times (Ob_i \times Oc_i)}{6}}$$

For each face in the mesh (i), defined by three vertices (a_i, b_i, c_i), the volume of the tetrahedron defined by i and the image origin (O) is calculated. The surface area is obtained from the sum of all triangle mesh areas and the volume from the sum of all tetrahedron volumes [21].

Finally, the multivariable analysis of T2w and ADC-derived SAVR showed statistical significance only for the latter ($p = 0.002$). At ROC curve analysis it obtained an AUC of 0.78 with a specificity and sensitivity, respectively of 97% and 56%.

Table 3
Clinical information of patient population. Data are presented as mean ± standard deviation.

	non-csPCa	csPCa
Number of patients	35	40
Age, median (interquartile range)	67 (8.5)	68 (8.25)
PSA (mean ± standard deviation)	6.6 ± 2.44	10.1 ± 9.20
Cognitive Targeted TRUS-Biopsy	21	21
Radical Prostatectomy	14	19
Gleason Score 3 + 3	17	–
Gleason Score 3 + 4	18	–
Gleason Score 4 + 3	–	17
Gleason Score 4 + 4	–	14
Gleason Score 4 + 5	–	3
Gleason Score 5 + 4	–	6

PSA: prostate-specific antigen; TRUS: transrectal ultrasound; csPCa: clinical significant prostate cancer.

4. Discussion

Radiomics, in possible combination with machine learning, has shown several interesting imaging applications in recent literature [27–31]. In particular, it has been applied to prostate MRI for staging, recurrence and tumor aggressiveness evaluation [19,20,32–34]. The results of our study showed that, among shape features extracted from MRI, the SAVR derived from ADC maps has the highest accuracy and appeared as the most promising tool in the discrimination of csPca from non-csPca, outperforming even previously proposed parameters such as lesion volume and maximum diameter. Indeed, a robust validation of

Table 2
Names and definitions of ten shape features extracted from both T2-weighted and ADC map images after index lesion segmentation.

Shape Feature Name	Definition
Maximum 3D Diameter	Maximum 3D diameter is defined as the largest pairwise Euclidean distance between tumor surface mesh vertices.
Major Axis	This feature yields the largest axis length of the VOI-enclosing ellipsoid.
Minor Axis	This feature yields the second-largest axis length of the VOI-enclosing ellipsoid.
Least Axis	This feature yields the smallest axis length of the VOI-enclosing ellipsoid.
Flatness	Flatness shows the relationship between the largest and smallest principal components in the VOI shape.
Elongation	Elongation shows the relationship between the two largest principal components in the VOI shape.
Sphericity	Measure of the roundness of the shape of the tumor region relative to a sphere.
Surface Area	Sum of the area of each triangle in the mesh.
Volume	The volume calculated from the triangle mesh of the VOI
Surface Area to Volume Ratio	Measure of the degree of tumor shape compactness (sphere-like shape).

VOI: volume of interest.

Table 4
Univariable analysis results for features extracted from T2-weighted images.

T2w Feature	non-csPCa	csPCa	O.R. (95% C.I.)	*p* value
Maximum 3D Diameter	13.11 (4.47 – 26.30)	19.59 (8.49 – 54.30)	1.1 (1.0-1.2)	0.0005
Major Axis	13.67 (6.47 – 24.59)	19 (9.15 – 46.85)	1.1 (1.0-1.2)	0.0018
Minor Axis	8.15 (1.67 – 14.84)	13.97 (4.18 – 38.76)	1.2 (1.1- 1.4)	< 0.0001
Least Axis	5.76 (0 – 10.49)	9.67 (3.43 – 21.48)	1.4 (1.2-1.7)	< 0.0001
Flatness	0.39 (0 – 0.65)	0.5 (0.24 – 0.8)	2.5 (0.8-7.7)	0.0003
Elongation	0.59 ± 0.16	0.73 ± 0.16	2.0 (0.8-5.1)	0.0004
Sphericity	0.80 (0.62 – 1.59)	0.76 (0.44 – 0.92)	0.01 (0.001-0.6)	0.0112
Surface Area	290.25 (33.18 – 1056.47)	856.27 (103.9 – 5040.23)	1.02 (1.01-1.03)	< 0.0001
Volume	332 (36 – 2016)	1528 (88 – 13616)	1.01 (1.00-1.03)	< 0.0001
Surface Area to Volume Ratio	0.87 ± 0.20	0.62 ± 0.22	0.01 (0.001-0.1)	< 0.0001

Data are expressed as mean ± standard deviation or median and range as appropriate.
csPCa, clinical significant prostate cancer; O.R.: odds ratio.

Table 5
Univariable analysis results for features extracted from ADC map images.

ADC Feature	non-csPCa	csPCa	O.R. (95% C.I.)	*p* value
Maximum 3D Diameter	10.77 (4.47 – 24.08)	18.49 (6.63 – 56.04)	1.2 (1.1 – 1.3)	< 0.0001
Major Axis	11.48 (5.91 – 23.17)	16.83 (7.52 – 43.59)	1.2 (1.1 – 1.3)	< 0.0001
Minor Axis	7.15 (2.47 – 16.8)	12.62 (4.79 – 34.65)	1.3 (1.1 – 1.4)	< 0.0001
Least Axis	5.44 (0 – 9.27)	9.14 (3.51 – 19.67)	1.4 (1.2 – 1.8)	< 0.0001
Flatness	0.49 (0 – 0.64)	0.51 (0.27 – 0.83)	11.1 (0.5 – 268.5)	0.1275
Elongation	0.69 ± 0.15	0.73 ± 0.16	2.8 (0.1 – 57.0)	0.5068
Sphericity	0.86 ± 0.13	0.76 ± 0.11	0.01 (0.001 – 0.44)	0.0103
Surface Area	250.73 (50.56 – 894.61)	662.25 (106.09-4233.64)	1.01 (1.00 – 1.02)	< 0.0001
Volume	296 (48 – 1736)	1096 (96 – 11384)	1.01 (1.00 – 1.02)	< 0.0001
Surface Area to Volume Ratio	0.91 ± 0.20	0.63 ± 0.22	0.0098 (0.0009 – 0.1073)	< 0.0001

Data are expressed as mean ± standard deviation or median and range as appropriate.
csPCa, clinical significant prostate cancer; O.R.: odds ratio.

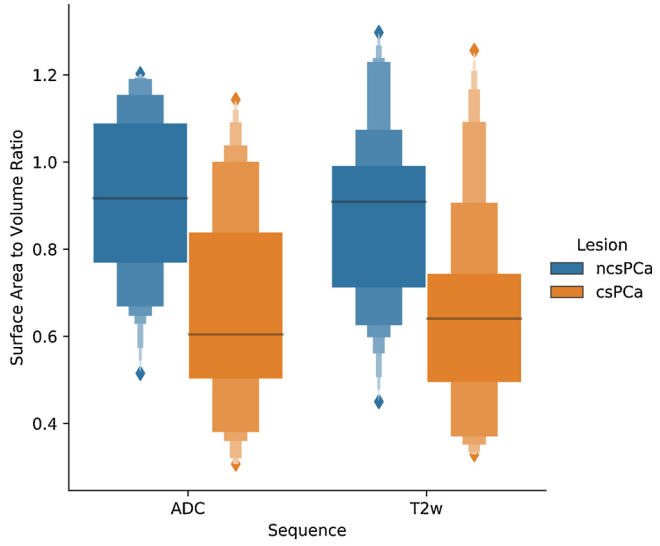

Fig. 3. Letter-value plot showing the distribution of lesion surface area to volume ratio in relation to extraction sequence and clinical significance.

MRI lesion volume led to its consideration within the latest version of PI-RADS as an independent indicator of clinical significance of PCa. Similarly, maximum diameter (with a cut-off of 15 mm) is one of the main criteria for defining the maximum lesion score in the same imaging guideline, together with signs of PCa extra-prostatic extension.

Our results show that more accurate shape parameters could be easily available once 3D lesion segmentation is performed. It should be noted that while drawing simple lines to estimate lesion diameters is an easier and faster task compared to 3D manual segmentation, prostate index lesions are usually relatively small and this process required, in our experience, less than 3 min on average. During the initial study design phase, MRI sequences used for segmentation (i.e. T2w and ADC map) were based on the dominant ones in the PI-RADSv2 [8]. The choice to exclude dynamic contrast enhanced (DCE) sequences was also due to their currently debated role [35–38].

Interestingly, the same shape feature, SAVR, resulted the most useful after multivariable analysis for csPCa discrimination in both T2w and ADC map images, strengthening our finding. We believe this also supports the hypothesis that shape features could be more reproducible independently of the imaging sequence from which they are extracted, unlike other radiomic parameters, facilitating their clinical applicability. It is also interesting to note that, overall, the SAVR derived from the ADC was more significant in the final multivariable analysis. While this might seem counterintuitive and unexpected, given the higher spatial resolution of T2w images, it could be due to the dominant nature of DWI and ADC in the peripheral zone, better reflecting PCa true extension in this area. Indeed, almost all of the lesions included in the study were located in the peripheral zone. Furthermore, DWI and more specifically ADC, can be considered the most robust and accurate sequence of prostate MR assessment, due to the higher contrast resolution between the lesion and the surrounding tissue [39]; this opens the door for a truly automated, even faster, post-processing pipeline from lesion segmentation to shape feature extraction. ADC mean values both in the form of ADC ratio and ADC 10th percentile have been previously proposed as reproducible quantitative markers to assess PCa aggressiveness [10,13,40,41]. More recently, Bonekamp et al. [42] did not find added value using a machine learning approach on radiomic data, including shape features, when compared to lesion mean ADC value. On the other hand, the authors exclusively assessed texture features via a random forest classifier without analyzing the merit of shape features directly, as done in the present study. Furthermore, a different cut-off value for the definition of csPCa was used (GS ≥ 3 + 4). It is also interesting to note that both the ADC mean and random forest achieved high sensitivity (respectively 90% and 97%) but lower specificity (respectively 62% and 58%), while using the ADC-derived SAVR, we obtained a

significantly higher specificity (97%). As specificity is a well-known limitation of prostate MRI, as also attested by the radiologist performance in the paper by Bonekamp and colleagues (sensitivity = 88%, specificity = 50%), the SAVR could better complement strength and limitations of MR prostatic imaging examination.

The results of our study revealed the robustness of geometric features and more specifically, ADC-derived SAVR emerged as the most powerful tool for identification of csPCa. We believe that shape features, being independent of voxel gray level, could be easily applied across scanners, with different field strengths and from various vendors when compared to other radiomic parameters derived from histograms and intensity value matrices.

The study presents several limitations. Low number of transitional zone PCa did not allow to perform a sub-analysis based on zonal anatomy. To guarantee an accurate annotation of MR images, we opted for a consensus reading for lesion segmentation, which prevented us from performing a reproducibility assessment analysis. The cognitive MRI target TRUS biopsy technique is prone to GS underestimation; however, several patients in our population underwent radical prostatectomy and final histopathology results, were used to assess index lesions GS. Finally, this was a single-center and single-scanner study, warranting future confirmation of our results in larger populations.

In conclusion, MRI index lesion shape features and in particular ADC-derived SAVR could aid in csPCa detection. Radiomics analysis through the quantitative assessment of geometric parameters has the potential to be used as a non-invasive test to predict GS for patients with csPCa; such analysis provides the additional benefit of automation, which can reduce human effort and cost whilst preventing patient morbidity and mortality associated with misdiagnosis and under/over-treatment.

Conflict of interest

None

References

[1] R.L. Siegel, K.D. Miller, A. Jemal, Cancer statistics, 2019, CA. Cancer J. Clin. 69 (2019) 7–34, https://doi.org/10.3322/caac.21551.

[2] S. Loeb, M.A. Bjurlin, J. Nicholson, T.L. Tammela, D.F. Penson, H.B. Carter, P. Carroll, R. Etzioni, Overdiagnosis and overtreatment of prostate cancer, Eur. Urol. 65 (2014) 1046–1055, https://doi.org/10.1016/j.eururo.2013.12.062.

[3] K.J.L. Bell, C. Del Mar, G. Wright, J. Dickinson, P. Glasziou, Prevalence of incidental prostate cancer: a systematic review of autopsy studies, Int. J. Cancer 137 (2015) 1749–1757, https://doi.org/10.1002/ijc.29538.

[4] T.J. Caverly, R.A. Hayward, E. Reamer, B.J. Zikmund-Fisher, D. Connochie, M. Heisler, A. Fagerlin, Presentation of benefits and harms in US cancer screening and prevention guidelines: systematic review, J. Natl. Cancer Inst. 108 (2016) 1–8, https://doi.org/10.1093/jnci/djv436.

[5] N. Mottet, J. Bellmunt, M. Bolla, E. Briers, M.G. Cumberbatch, M. De Santis, N. Fossati, T. Gross, A.M. Henry, S. Joniau, T.B. Lam, M.D. Mason, V.B. Matveev, P.C. Moldovan, R.C.N. van den Bergh, T. Van den Broeck, H.G. van der Poel, T.H. van der Kwast, O. Rouvière, I.G. Schoots, T. Wiegel, P. Cornford, EAU-ESTRO-SIOG guidelines on prostate cancer. Part 1: screening, diagnosis, and local treatment with curative intent, Eur. Urol. 71 (2017) 618–629, https://doi.org/10.1016/j.eururo.2016.08.003.

[6] J.R. Stark, S. Perner, M.J. Stampfer, J.A. Sinnott, S. Finn, A.S. Eisenstein, J. Ma, M. Fiorentino, T. Kurth, M. Loda, E.L. Giovannucci, M.A. Rubin, L.A. Mucci, Gleason score and lethal prostate cancer: does 3 + 4 = 4 + 3? J. Clin. Oncol. 27 (2009) 3459–3464, https://doi.org/10.1200/JCO.2008.20.4669.

[7] H.U. Ahmed, A. El-Shater Bosaily, L.C. Brown, R. Gabe, R. Kaplan, M.K. Parmar, Y. Collaco-Moraes, K. Ward, R.G. Hindley, A. Freeman, A.P. Kirkham, R. Oldroyd, C. Parker, M. Emberton, Diagnostic accuracy of multi-parametric MRI and TRUS biopsy in prostate cancer (PROMIS): a paired validating confirmatory study, Lancet 389 (2017) 815–822, https://doi.org/10.1016/S0140-6736(16)32401-1.

[8] J.O. Barentsz, J.C. Weinreb, S. Verma, H.C. Thoeny, C.M. Tempany, F. Shtern, A.R. Padhani, D. Margolis, K.J. Macura, M.A. Haider, F. Cornud, P.L. Choyke, Synopsis of the PI-RADS v2 guidelines for multiparametric prostate magnetic resonance imaging and recommendations for use, Eur. Urol. 69 (2016) 41–49, https://doi.org/10.1016/j.eururo.2015.08.038.

[9] M.G. Schouten, M. van der Leest, M. Pokorny, M. Hoogenboom, J.O. Barentsz, L.C. Thompson, J.J. Fütterer, Why and where do We miss significant prostate cancer with multi-parametric magnetic resonance imaging followed by magnetic resonance-guided and transrectal ultrasound-guided biopsy in biopsy-naïve men? Eur. Urol. 71 (2017) 896–903, https://doi.org/10.1016/j.eururo.2016.12.006.

[10] S. Lee, Y.T. Oh, D.C. Jung, N.H. Cho, Y.D. Choi, S.Y. Park, Combined analysis of biparametric MRI and prostate-specific antigen density: role in the prebiopsy diagnosis of gleason score 7 or Greater prostate cancer, Am. J. Roentgenol. 211 (2018) W166–W172, https://doi.org/10.2214/AJR.17.19253.

[11] Y. Yanai, T. Kosaka, H. Hongo, K. Matsumoto, T. Shinojima, E. Kikuchi, A. Miyajima, R. Mizuno, S. Mikami, M. Jinzaki, M. Oya, Evaluation of prostate-specific antigen density in the diagnosis of prostate cancer combined with magnetic resonance imaging before biopsy in men aged 70 years and older with elevated PSA, Mol. Clin. Oncol. (2018) 656–660, https://doi.org/10.3892/mco.2018.1725.

[12] R. Cuocolo, A. Stanzione, G. Rusconi, M. Petretta, A. Ponsiglione, F. Fusco, N. Longo, F. Persico, S. Cocozza, A. Brunetti, M. Imbriaco, PSA-density does not improve bi-parametric prostate MR detection of prostate cancer in a biopsy naïve patient population, Eur. J. Radiol. 104 (2018) 64–70, https://doi.org/10.1016/j.ejrad.2018.05.004.

[13] O.F. Donati, Y. Mazaheri, A. Afaq, H.A. Vargas, J. Zheng, C.S. Moskowitz, H. Hricak, O. Akin, Prostate cancer aggressiveness: assessment with whole-lesion histogram analysis of the apparent diffusion coefficient, Radiology 271 (2014) 143–152, https://doi.org/10.1148/radiol.13130973.

[14] T. Tamada, V. Prabhu, J. Li, J.S. Babb, S.S. Taneja, A.B. Rosenkrantz, Prostate cancer: diffusion-weighted MR imaging for detection and assessment of aggressiveness—comparison between conventional and kurtosis models, Radiology 284 (2017) 100–108, https://doi.org/10.1148/radiol.2017162321.

[15] R.J. Gillies, P.E. Kinahan, H. Hricak, Radiomics: images are more than pictures, they are data, Radiology 278 (2016) 563–577, https://doi.org/10.1148/radiol.2015151169.

[16] F. Khalvati, A. Wong, M.A. Haider, Automated prostate cancer detection via comprehensive multi-parametric magnetic resonance imaging texture feature models, BMC Med. Imaging 15 (2015) 1–14, https://doi.org/10.1186/s12880-015-0069-9.

[17] S.B. Ginsburg, S.E. Viswanath, B.N. Bloch, N.M. Rofsky, E.M. Genega, R.E. Lenkinski, A. Madabhushi, Novel PCA-VIP scheme for ranking MRI protocols and identifying computer-extracted MRI measurements associated with central gland and peripheral zone prostate tumors, J. Magn. Reson. Imaging 41 (2015) 1383–1393, https://doi.org/10.1002/jmri.24676.

[18] G.J.S. Litjens, R. Elliott, N.N. Shih, M.D. Feldman, T. Kobus, C. Hulsbergen-van de Kaa, J.O. Barentsz, H.J. Huisman, A. Madabhushi, Computer-extracted features can distinguish noncancerous confounding disease from prostatic adenocarcinoma at multiparametric MR imaging, Radiology 278 (2016) 135–145, https://doi.org/10.1148/radiol.2015142856.

[19] G. Nketiah, M. Elschot, E. Kim, J.R. Teruel, T.W. Scheenen, T.F. Bathen, K.M. Selnæs, T2-weighted MRI-derived textural features reflect prostate cancer aggressiveness: preliminary results, Eur. Radiol. 27 (2017) 3050–3059, https://doi.org/10.1007/s00330-016-4663-1.

[20] A. Stanzione, R. Cuocolo, S. Cocozza, V. Romeo, F. Persico, F. Fusco, N. Longo, A. Brunetti, M. Imbriaco, Detection of extraprostatic extension of cancer on biparametric MRI combining texture analysis and machine learning: preliminary results, Acad. Radiol. (2019) 1–7, https://doi.org/10.1016/j.acra.2018.12.025.

[21] W.E. Lorensen, H.E. Cline, Marching cubes: a high resolution 3D surface construction algorithm, ACM SIGGRAPH Comput. Graph. (1987), https://doi.org/10.1145/37402.37422.

[22] S. Krishna, N. Schieda, M.D. McInnes, T.A. Flood, R.E. Thornhill, Diagnosis of transition zone prostate cancer using T2-weighted (T2W) MRI: comparison of subjective features and quantitative shape analysis, Eur. Radiol. 29 (2019) 1133–1143, https://doi.org/10.1007/s00330-018-5664-z.

[23] T.A. Stamey, F.S. Freiha, J.E. McNeal, E.A. Redwine, A.S. Whittemore, H. -P Schmid, Localized prostate cancer. Relationship of tumor volume to clinical significance for treatment of prostate cancer, Cancer 71 (1993) 933–938.

[24] P.A. Yushkevich, J. Piven, H.C. Hazlett, R.G. Smith, S. Ho, J.C. Gee, G. Gerig, User-guided 3D active contour segmentation of anatomical structures: significantly improved efficiency and reliability, Neuroimage 31 (2006) 1116–1128, https://doi.org/10.1016/j.neuroimage.2006.01.015.

[25] J.J.M. Van Griethuysen, A. Fedorov, C. Parmar, A. Hosny, N. Aucoin, V. Narayan, R.G.H. Beets-Tan, J.C. Fillion-Robin, S. Pieper, H.J.W.L. Aerts, Computational radiomics system to decode the radiographic phenotype, Cancer Res. 77 (2017) e104–e107, https://doi.org/10.1158/0008-5472.CAN-17-0339.

[26] J.A. Hanley, B.J. McNeil, A method of comparing the areas under receiver operating characteristic curves derived from the Same cases, Radiology 148 (1983) 839–843, https://doi.org/10.1148/radiology.148.3.6878708.

[27] G. Choy, O. Khalilzadeh, M. Michalski, S. Do, A.E. Samir, O.S. Pianykh, J.R. Geis, P.V. Pandharipande, J.A. Brink, K.J. Dreyer, Current applications and future impact of machine learning in radiology, Radiology 288 (2018) 318–328, https://doi.org/10.1148/radiol.2018171820.

[28] C.A. Sarkiss, I.M. Germano, Machine learning in neuro-oncology: can data analysis from 5346 patients change decision-making paradigms? World Neurosurg. 124 (2019) 287–294, https://doi.org/10.1016/j.wneu.2019.01.046.

[29] M. Sollini, L. Cozzi, A. Chiti, M. Kirienko, Texture analysis and machine learning to characterize suspected thyroid nodules and differentiated thyroid cancer: where do we stand? Eur. J. Radiol. 99 (2018) 1–8, https://doi.org/10.1016/j.ejrad.2017.12.004.

[30] V. Romeo, S. Maurea, R. Cuocolo, M. Petretta, P.P. Mainenti, F. Verde, M. Coppola, S. Dell'Aversana, A. Brunetti, Characterization of adrenal lesions on unenhanced MRI using texture analysis: a machine-learning approach, J. Magn. Reson. Imaging 48 (2018) 198–204, https://doi.org/10.1002/jmri.25954.

[31] M. Imbriaco, R. Cuocolo, Does texture analysis of MR images of breast tumors help predict response to treatment? Radiology 286 (2018) 421–423, https://doi.org/10.

1148/radiol.2017172454.
[32] S. Krishna, C.S. Lim, M.D.F. McInnes, T.A. Flood, W.M. Shabana, R.S. Lim, N. Schieda, Evaluation of MRI for diagnosis of extraprostatic extension in prostate cancer, J. Magn. Reson. Imaging 47 (2018) 176–185, https://doi.org/10.1002/jmri.25729.
[33] A. Wibmer, H. Hricak, T. Gondo, K. Matsumoto, H. Veeraraghavan, D. Fehr, J. Zheng, D. Goldman, C. Moskowitz, S.W. Fine, V.E. Reuter, J. Eastham, E. Sala, H.A. Vargas, Haralick texture analysis of prostate MRI: utility for differentiating non-cancerous prostate from prostate cancer and differentiating prostate cancers with different gleason scores, Eur. Radiol. 25 (2015) 2840–2850, https://doi.org/10.1007/s00330-015-3701-8.
[34] D. Fehr, H. Veeraraghavan, A. Wibmer, T. Gondo, K. Matsumoto, H.A. Vargas, E. Sala, H. Hricak, J.O. Deasy, Automatic classification of prostate cancer gleason scores from multiparametric magnetic resonance images, Proc. Natl. Acad. Sci. 112 (2015) E6265–E6273, https://doi.org/10.1073/pnas.1505935112.
[35] Y. Kaji, K. Inamura, Diagnostic ability with abbreviated biparametric and full multiparametric prostate MR imaging: Is the use of PI-RADS version 2 appropriate for comparison? Radiology 286 (2018) 726–727, https://doi.org/10.1148/radiol.2017172265.
[36] A. Stanzione, R. Cuocolo, S. Cocozza, M. Imbriaco, Predicting prognosis with biparametric prostate imaging: one step at a time, Clin. Genitourin. Cancer 16 (2018) e977–e978, https://doi.org/10.1016/j.clgc.2018.04.006.
[37] A. Stanzione, S. Cocozza, R. Cuocolo, M. Imbriaco, Biparametric prostate MR imaging protocol: time to revise PI-RADS version 2? Radiology 287 (2018) 1082, https://doi.org/10.1148/radiol.2018180292.
[38] A. Stanzione, M. Imbriaco, S. Cocozza, F. Fusco, G. Rusconi, C. Nappi, V. Mirone, F. Mangiapia, A. Brunetti, A. Ragozzino, N. Longo, Biparametric 3T magentic resonance imaging for prostatic cancer detection in a biopsy-naïve patient population: a further improvement of PI-RADS v2? Eur. J. Radiol. 85 (2016) 2269–2274, https://doi.org/10.1016/j.ejrad.2016.10.009.
[39] A. Chatterjee, G. Watson, E. Myint, P. Sved, M. McEntee, R. Bourne, changes in epithelium, stroma, and lumen space correlate more strongly with gleason pattern and are stronger predictors of prostate ADC changes than cellularity metrics, Radiology 277 (2015) 751–762, https://doi.org/10.1148/radiol.2015142414.
[40] A. Hoang Dinh, C. Melodelima, R. Souchon, J. Lehaire, F. Bratan, F. Mège-Lechevallier, A. Ruffion, S. Crouzet, M. Colombel, O. Rouvière, Quantitative analysis of prostate multiparametric MR images for detection of aggressive prostate cancer in the peripheral zone: a multiple imager study, Radiology 280 (2016) 117–127, https://doi.org/10.1148/radiol.2016151406.
[41] Y. Peng, Y. Jiang, T. Antic, M.L. Giger, S.E. Eggener, A. Oto, Validation of quantitative analysis of multiparametric prostate MR images for prostate cancer detection and aggressiveness assessment: a Cross-imager study, Radiology 271 (2014) 461–471, https://doi.org/10.1148/radiol.14131320.
[42] D. Bonekamp, S. Kohl, M. Wiesenfarth, P. Schelb, J.P. Radtke, M. Götz, P. Kickingereder, K. Yaqubi, B. Hitthaler, N. Gählert, T.A. Kuder, F. Deister, M. Freitag, M. Hohenfellner, B.A. Hadaschik, H.-P. Schlemmer, K.H. Maier-Hein, Radiomic machine learning for characterization of prostate lesions with MRI: comparison to ADC values, Radiology 289 (2018) 128–137, https://doi.org/10.1148/radiol.2018173064.